EPJ Web of Conferences **137**, 03018 (2017) DOI: 10.1051/epjconf/201713703018
XIIth Quark Confinement & the Hadron Spectrum

Three-gluon Green functions: low-momentum instanton dominance and zero-crossing

J. Rodríguez-Quintero[1,2,a], A. Athenodorou[3], D. Binosi[4], Ph. Boucaud[5], F. De Soto[6], J. Papavassiliou[7], and S. Zafeiropoulos[8]

[1]*Department of Integrated Sciences; University of Huelva, E-21071 Huelva, Spain.*
[2]*CAFPE; Universidad of Granada; E-18071 Granada, Spain.*
[3]*Department of Physics, University of Cyprus, POB 20537, 1678 Nicosia, Cyprus*
[4]*ECT*, Villa Tambosi, Strada delle Tabarelle 286, I-38050 Villazzano (TN), Italy.*
[5]*LPT (UMR8627), CNRS, Univ. Paris-Sud, Université Paris-Saclay, 91405 Orsay, France*
[6]*Dpto. Sistemas Físicos, Químicos y Naturales, Univ. Pablo de Olavide, 41013 Sevilla, Spain*
[7]*Department of Theoretical Physics and IFIC, University of Valencia-CSIC, E-46100, Valencia, Spain.*
[8]*Institut für Theoretische Physik, Goethe-Universität Frankfurt, Max-von-Laue-Str. 1, 60438 Frankfurt am Main, Germany*

Abstract. We will report on a some efforts recently made in order to gain a better understanding of some IR properties of the 3-point gluon Green function by following both lattice and continuum QCD approaches.

1 Introduction

The ongoing intense exploration of the infrared (IR) sector of Quantum Chromodynamics (QCD) has led into the detailed scrutiny of the fundamental Green's functions of the theory using large-volume lattice simulations (see, for instance [1–5], together with a variety of continuum approaches (see, for instance [6–12]). Even though off-shell Green's functions are not physical quantities, given their explicit dependence on the gauge-fixing parameter and the renormalization scheme, they encode valuable information on fundamental nonperturbative phenomena such as confinement, chiral symmetry breaking, and dynamical mass generation, and constitute the basic building blocks of symmetry-preserving formalisms that aim at a veracious description of hadron phenomenology (see, for instance [13–18]).

Two very recent papers [19, 20] made an effort to investigate further a few key features of the 3-point gluon Green function by both exploiting up-to-date lattice data and accomodating the results within alternative continuum approaches. We will briefly review here these two works.

2 Connected and 1-PI 3-gluon Green's functions

Let us first properly define the connected and the usual 1-particle irreducible (1-PI) 3-gluon Green functions and describe then how they can be nonperturbatively obtained.

[a]e-mail: jose.rodriguez@dfaie.uhu.es

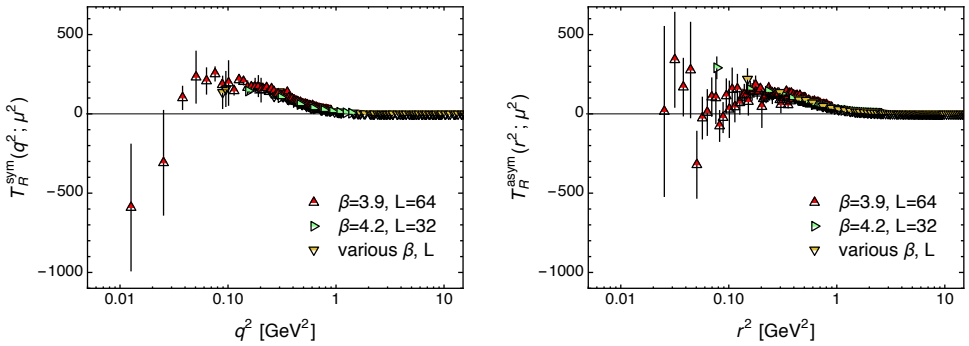

Figure 1. (color online) Lattice results for the renormalized connected form factor T_R in the symmetric (left) and asymmetric (right) momentum configuration. For both data sets the renormalization point $\mu = 4.3$ GeV was chosen. The same scale is used in both plots which reveals the similar behavior of the two form factors.

2.1 Definitions and generalities

The connected three-gluon vertex is defined as the correlation function ($q + r + p = 0$)

$$\mathcal{G}^{abc}_{\alpha\mu\nu}(q,r,p) = \langle A^a_\alpha(q) A^b_\mu(r) A^c_\nu(p)\rangle = f^{abc}\mathcal{G}_{\alpha\mu\nu}(q,r,p), \tag{1}$$

where the sub (super) indices represent Lorentz (color) indices and the average $\langle\cdot\rangle$ indicates functional integration over the gauge space. In terms of the 1-PI function, one has

$$\mathcal{G}_{\alpha\mu\nu}(q,r,p) = g\Gamma_{\alpha'\mu'\nu'}(q,r,p)\Delta_{\alpha'\alpha}(q)\Delta_{\mu'\mu}(r)\Delta_{\nu'\nu}(p), \tag{2}$$

with g the strong coupling constant. In the Landau gauge, the transversality of the gluon propagator, *viz.*,

$$\Delta^{ab}_{\mu\nu}(q) = \langle A^a_\mu(q) A^b_\nu(-q)\rangle = \delta^{ab}\Delta(p^2)P_{\mu\nu}(q), \tag{3}$$

where $P_{\mu\nu}(q) = \delta_{\mu\nu} - q_\mu q_\nu/q^2$, implies directly that $\mathcal{G}$ is totally transverse: $q\cdot\mathcal{G} = r\cdot\mathcal{G} = p\cdot\mathcal{G} = 0$.

In what follows we will consider two special momenta configurations. The first one is the so-called symmetric configuration, in which $q^2 = r^2 = p^2$ and $q\cdot r = q\cdot p = r\cdot p = -q^2/2$; in this case, there are only two totally transverse tensors, namely

$$\begin{aligned}\lambda^{\rm tree}_{\alpha\mu\nu}(q,r,p) &= \Gamma^{(0)}_{\alpha'\mu'\nu'}(q,r,p)P_{\alpha'\alpha}(q)P_{\mu'\mu}(r)P_{\nu'\nu}(p),\\ \lambda^{S}_{\alpha\mu\nu}(q,r,p) &= (r-p)_\alpha(p-q)_\mu(q-r)_\nu/r^2,\end{aligned} \tag{4}$$

where $\Gamma^{(0)}_{\alpha\mu\nu}$ is the usual tree-level vertex. Indicating with $S^{\rm sym}$ and $T^{\rm sym}$ (respectively, $\Gamma^{\rm sym}_S$ and $\Gamma^{\rm sym}_T$) the corresponding form factors in the decomposition of $\mathcal{G}$ (respectively, Γ) in this momentum configuration, Eq. (2) implies the relation

$$\begin{aligned}T^{\rm sym}(q^2) &= g\,\Gamma^{\rm sym}_T(q^2)\,\Delta^3(q^2),\\ S^{\rm sym}(q^2) &= g\,\Gamma^{\rm sym}_S(q^2)\,\Delta^3(q^2).\end{aligned} \tag{5}$$

In particular, the $T^{\rm sym}$ form factor can be projected out through

$$T^{\rm sym}(q^2) = \left. \frac{W_{\alpha\mu\nu}(q,r,p)\,\mathcal{G}_{\alpha\mu\nu}(q,r,p)}{W_{\alpha\mu\nu}(q,r,p)W_{\alpha\mu\nu}(q,r,p)} \right|_{\rm sym}, \tag{6}$$

with $W = \lambda^{\rm tree} + \lambda^S/2$.

The second configuration we will study, which will be called 'asymmetric' in what follows, is defined by taking the $q \to 0$ limit, while imposing at the same time the condition $r^2 = p^2 = -p\cdot r$. In this configuration $\lambda^S_{\alpha\mu\nu} \sim r_\alpha r_\mu r_\nu$ becomes totally longitudinal, and the only transverse tensor one can construct is obtained by the $q \to 0$ limit of $\lambda^{\rm tree}$ (obviously omitting the q projector), *i.e.*,

$$\lambda^{\rm tree}_{\alpha\mu\nu}(0,r,-r) = 2r_\alpha P_{\mu\nu}(r). \tag{7}$$

Thus one is left with a single form factor, which can be projected out through

$$\begin{aligned} T^{\rm asym}(r^2) &= \left. \frac{W_{\alpha\mu\nu}(q,r,p)\,\mathcal{G}_{\alpha\mu\nu}(q,r,p)}{W_{\alpha\mu\nu}(q,r,p)W_{\alpha\mu\nu}(q,r,p)} \right|_{\rm asym} \\ &= g\,\Gamma^{\rm asym}_T(r^2)\,\Delta(0)\,\Delta^2(r^2), \end{aligned} \tag{8}$$

where now $W = \lambda^{\rm tree}$.

All the quantities defined so far are bare, and a dependence on the regularization cut-off must be implicitly understood. Within a given renormalization procedure, the renormalized Green's functions are calculated in terms of the renormalized fields $A_R = Z_A^{-1/2}A$, so that

$$\begin{aligned} \Delta_R(q^2;\mu^2) &= Z_A^{-1}(\mu^2)\,\Delta(q^2), \\ T^{\rm sym}_R(q^2;\mu^2) &= Z_A^{-3/2}(\mu^2)T^{\rm sym}(q^2), \end{aligned} \tag{9}$$

and similarly for the asymmetric configuration. Within the MOM scheme that we will employ, one then requires that all the Green's functions take their tree-level expression at the subtraction point, namely

$$\begin{aligned} \Delta_R(q^2;q^2) &= Z_A^{-1}(q^2)\,\Delta(q^2) = 1/q^2, \\ T^{\rm sym}_R(q^2;q^2) &= Z_A^{-3/2}(q^2)\,T^{\rm sym}(q^2) = g^{\rm sym}_R(q^2)/q^6. \end{aligned} \tag{10}$$

The first equation yields the renormalization constant Z_A as a function of the bare propagator, which when substituted into the second equation provides a renormalization group invariant definition of the three-gluon MOM running coupling [21, 22]:

$$g^{\rm sym}(q^2) = q^3\,\frac{T^{\rm sym}(q^2)}{[\Delta(q^2)]^{3/2}} = q^3\,\frac{T^{\rm sym}_R(q^2;\mu^2)}{[\Delta_R(q^2;\mu^2)]^{3/2}}. \tag{11}$$

In the asymmetric configuration the relation is slightly different, as in this case one has

$$T^{\rm asym}_R(r^2;r^2) = Z_A^{-3/2}(r^2)\,T^{\rm asym}(r^2) = \Delta_R(0;q^2)\,g^{\rm asym}_R(r^2)/r^4, \tag{12}$$

implying

$$g^{\rm asym}(r^2) = r^3\,\frac{T^{\rm asym}(r^2)}{[\Delta(r^2)]^{1/2}\Delta(0)} = r^3\,\frac{T^{\rm asym}_R(r^2;\mu^2)}{[\Delta_R(r^2;\mu^2)]^{1/2}\Delta_R(0;\mu^2)}. \tag{13}$$

Finally, in both cases the above equations yield for the 1-PI form factors the relation

$$g^i(\mu^2)\,\Gamma^i_{T,R}(\ell^2;\mu^2) = \frac{g^i_R(\ell^2)}{[\ell^2\Delta(\ell^2;\mu^2)]^{3/2}}, \tag{14}$$

where i indicates either the symmetric or the asymmetric momentum configuration, and, correspondingly, $\ell^2 = q^2,\ r^2$.

This latter result is of special interest because it establishes a connection between the three-gluon MOM running coupling, which many lattice and continuum studies have paid attention to, and the vertex function of the amputated three-gluon Green's function, a fundamental ingredient within the tower of (truncated) SDEs addressing non-perturbative QCD phenomena. In fact, these quantities are related only by the gluon propagator Δ, which, after the intensive studies of the past decade, is very well understood and accurately known.

2.2 Lattice results

The matrix elements in Eqs. (1) and (3) can be obtained as, respectively, 2- and 3-points gluon correlation functions from the lattice and, after the appropriate projections described in the previous subsection, be applied to yield the 1-PI and connected 3-gluon form factors, related by Eqs. (5) and (8). In order to do so, in [19], quenched SU(3) configurations at several large volumes and different bare couplings β, obtained employing the tree-level Symanzik gauge action, were exploited: 220 configurations at $\beta = 4.20$ for a hypercubic lattice of length $L = 32$ (corresponding to a physical volume of 4.5^4 fm^4) and 900 configurations at $\beta = 3.90$ for a $L = 64$ lattice (physical volume 15.6^4 fm^4). The data extracted from these new gauge configurations have been supplemented with the one derived from the old configurations of [23], obtained using the Wilson gauge action at several β (ranging from 5.6 to 6.0), lattices (from $L = 24$ to $L = 32$) and physical volumes (from 2.4^4 to 5.9^4 fm^4).

In Fig. 1 we plot the form factor T renormalized at $\mu = 4.3$ GeV for both the symmetric (left panel) and asymmetric (right panel) momentum configuration. In the symmetric case $T^{\rm sym}_R$ displays a zero crossing located in the IR region around 0.1–0.2 GeV, after which the data seems to indicate that some sort of divergent behavior manifests itself. In the asymmetric case the situation looks less clear as data are noisier, as a result of forcing one momentum to vanish.

Then, once the connected 3-gluon form factors and gluon propagators obtained, Eqs. (11) and (13) allow us for the computation of the running coupling in different schemes. In the next section, we will focus, in particular, in the first one corresponding to the so-called MOM symmetric 3-gluon coupling. Apart from the previous gauge-field lattice configurations, for the coupling analysis and comparison purpose, we have furthermore exploited the unquenched lattice configurations with two degenerate light dynamical (u and d) and two heavier (s and c) flavors which made possible a successful determination of the $\overline{\rm MS}$ running coupling at the Z^0-mass scale [24].

3 Analysis of results

We will now briefly describe the analysis of results already made and presented (including many more details) in refs. [19, 20], mainly addressed to understand a few striking features taking place in the low-momentum domain.

3.1 Gluon Green's function free of quantum fluctuations

First, as described in [19], the lattice-gauge fields have been deprived from their short-distance UV fluctuations by applying the so-called Wilson flow technique, which has proven to be an essential tool

in modern non-perturbative studies of QCD [25, 26]. Then, the *flown* gauge fields have been again projected to Landau-gauge and used to compute 3-gluon form factors and couplings, as previously described. The so-obtained results have finally been analyzed in terms of the quasi-classical solutions of the SU(3) gauge action.

The gauge-field classical solution from an ensemble of instantons, B^a_μ, can be described in terms of the coined as ratio-ansatz [27] which, specially far away from all the instantons' centers or in the vicinity of one of them, can be approximated by

$$g_0\, B^a_\mu(\mathbf{x}) = 2\sum_i R^{a\alpha}_{(i)}\, \overline{\eta}^\alpha_{\mu\nu}\, \frac{y^\nu_i}{y^2_i}\, \phi_{\rho_i}\left(\frac{|y_i|}{\rho_i}\right)\,; \tag{15}$$

where $y_i = (x - z^i)$ and $\overline{\eta}^\alpha_{\mu\nu}$ is the 't Hooft symbol, that should be replaced by $\eta^\alpha_{\mu\nu}$ when summing over anti-instantons as $i = A$. $R^{a\alpha}_{(i)}$ represents the color rotations embedding the canonical SU(2) instanton solution in the SU(3) gauge group (*i.e.,* $\alpha = 1, 2, 3$ and $a = 1, 2, \ldots 8$). provided that the profile function ϕ behaves as

$$\phi_\rho(z) = \begin{cases} \dfrac{f(\rho z)}{f(\rho z) + z^2} \simeq \dfrac{1}{1+z^2} & z \ll 1 \\ \dfrac{f(\rho z)}{z^2} & z \gg 1 \end{cases}\,, \tag{16}$$

where $f(z)$ is the shape function which can be obtained by minimizing the action per particle for some statistical ensemble of instantons defining the semiclassical background. This function essentially drives the large-distance behavior of the gauge field due to one-instanton contributions and incorporates also the nonlinear effects resulting from the average classical interaction of the other instantons in the background. According to [28], this shape function and the large-distance drop can be approximated as being independent of the low-distance scale ρ fixing the instanton size. However, the profile function ϕ, defined to match both large- and low-distance behaviors, needs to break this scale independence as we did explicitly in Eq. (16).

Then, as explained in [23], the gauge-field Green functions can be semi-classically obtained within the instanton background as

$$g^m_0 G^{(m)}(k^2) = \frac{k^{2-m}}{m4^{m-1}}\, n\, \langle\, \rho^{3m} I^m(k\rho)\, \rangle \tag{17}$$

where the compact notation $G^{(3)} = T^{\rm sym}$ and $G^{(2)} = \Delta$ is used, n is the instanton density,

$$I(s) \;=\; \frac{8\pi^2}{s}\int_0^\infty z dz J_2(sz)\phi(z) \tag{18}$$

and $\langle \ldots \rangle$ expresses the average over the distribution of instantons within the statistical ensemble defining the background. Thus, (11) gives for the symmetric running coupling in the instanton field:

$$\alpha^{\rm sym}(k^2) = \frac{(g^{\rm sym}(k^2))^2}{4\pi} = \frac{k^6}{4\pi}\frac{\left(G^{(3)}(k^2)\right)^2}{\left(G^{(2)}(k^2)\right)^3} = \frac{k^4}{18\pi n}\frac{\langle\rho^9 I^3(k\rho)\rangle^2}{\langle\rho^6 I^2(k\rho)\rangle^3}\,. \tag{19}$$

Whichever the shape function $f(x)$ might be, the topological condition $f(0) = 1$ guarantees that $I(s)$=$18\pi^2/s^3$ when $s \to \infty$ and then

$$\frac{\langle\rho^9 I^3(k\rho)\rangle^2}{\langle\rho^6 I^2(k\rho)\rangle^3} \simeq 1 + O\left(\frac{\delta\rho^2}{k^2\bar{\rho}^4}\right)\,, \tag{20}$$

where $\bar{\rho} = \sqrt{\langle\rho^2\rangle}$ and $\delta\rho^2 = \langle(\rho - \rho)^2\rangle$ stand for the mean square width of the radii distribution. On the other hand, only relying on the sufficient cut-off of $f(x)$ at large distances, one would be left with

$$\frac{\langle\rho^9 I^3(k\rho)\rangle^2}{\langle\rho^6 I^2(k\rho)\rangle^3} \simeq 1 + 48\frac{\delta\rho^2}{\bar{\rho}^2} + O\left(k^2\delta\rho^2, \frac{\delta\rho^4}{\bar{\rho}^4}\right). \tag{21}$$

for the low-momentum domain. Had we considered a zero width for the radii distribution, the coupling defined by Eq. (19) would plainly behave as a scale-independent k^4-power law for all momenta.

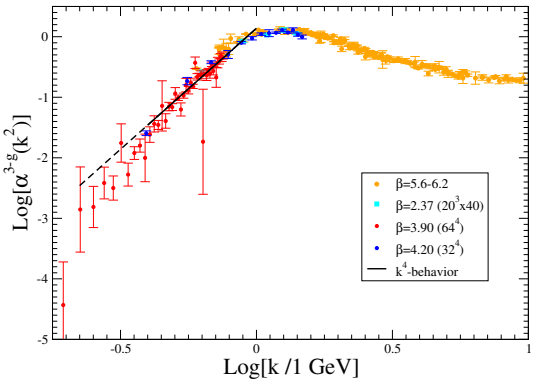

Figure 2. The MOM three-gluon coupling defined in Eq. (11) obtained from all the different quenched lattice simulations described in the text.

As can be seen in in 2, the coupling obtained with Eq. (11) for all quenched *non-flown* gauge fields behaves accordingly to (21), at low momenta. It should be first noticed that, as corresponding to the RGI nature of the RHS of Eq. (11), all the data from different simulations with different actions and set-up's show a very good physical scaling. However, the main feature to be underlined is that, before applying the Wilson flow, a momentum scale, lying around 1 GeV (in the ballpark of $\Lambda_{\rm QCD}$), separates clearly two regimes, the one above this scale where quantum corrections manage to build the well-known perturbative logarithmic running and that below, where the power law from Eq. (19) appears to rise. The intercept of the low-momenta logarithmic line, as is highlighted by the above-mentioned good scaling, is a physical quantity, and can be very well used for a cheap calibration of the lattice spacing. Its value estimated from data is 1.44 GeV^{-4} and, by neglecting the radii distribution width, one would be left for the instanton density with $n = 7.7(1)$ fm^{-4}.

We have now considered only the quenched lattice configurations at $\beta = 4.20$ and the unquenched ones at $\beta = 1.95$, applied the Wilson flow technique which is designed to destroy all the short-distance fluctuations in the gluon correlations, computed again the symmetric running coupling and displayed the results displayed in Fig. 3. The characteristic diffusion length of the Wilson flow is controlled for a parameter, the flow time: the longer is the former the larger the latter. Three different flow times (τ=4,8 and 15 in lattice units) have been considered and the resulting behaviours at both low- and large-momentum domains can be strinkingly well explained by Eqs. (19-21). Additionally, the intercepts of the large-momentum lines provide with an estimate for the instanton density at different flow times: $n = 3.5(1), 1.75(4), 0.98(5)$ fm^{-4} at $\tau = 4, 8, 15$, for the quenched case; and $n = 6.8(5), 3.0(2)$ fm^{-4} at $\tau = 8, 15$, for the unquenched case. Furthermore, the larger the flow time the lower momenta the non-enhanced linear behavior of Eq. (20) appears to extend down for. This suggests that the instanton size grows with the flow time, at least in a first stage, when the instanton density is as high as we obtain and the instanton-anti-instanton annihilation is the mechanism dominating the evolution of the quasi-classical solutions.

On the other hand, according to Eq. (21), wherever the momenta satisfy $k^2\delta\rho^2 \ll 1$, the intercept for the low-momentum line is shifted up by $\log(1 + 48\delta\rho^2/\bar{\rho}^2) \simeq 48/\ln 10\ \delta\rho^2/\bar{\rho}^2$. Therefore, one

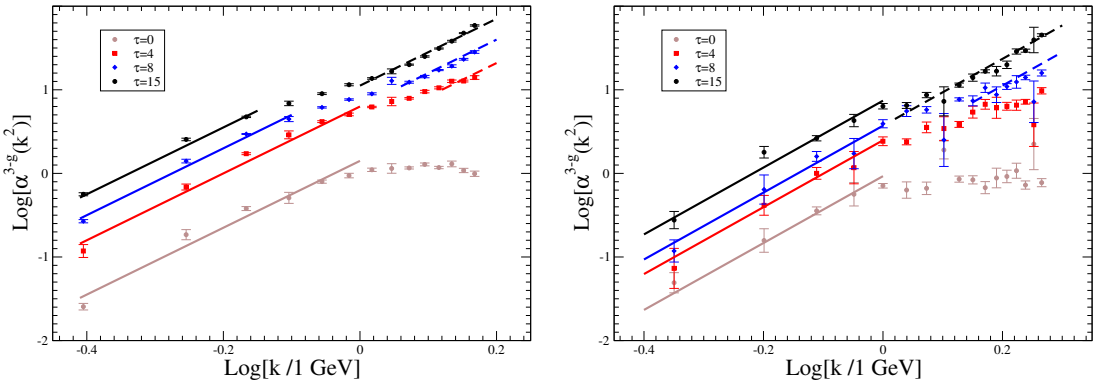

Figure 3. The MOM three-gluon coupling defined in Eq. (11) obtained from quenched data with $\beta = 4.20$ (left panel) and unquenched with $\beta = 1.95$ (right panel) lattice simulations at different flow times.

can get $\delta\rho^2/\bar{\rho}^2 \simeq 0.014$ (quenched) and 0.013 (unquenched), from the comparison of the intercepts in Fig. 3. These numbers compare very well with independent estimates obtained by direct instanton detection after cooling lattice gauge configurations in the quenched approximation [19]. Finally, at zero flow time, the unquenched instanton density can be estimated to be 1.55 times larger than the quenched one, if both unknown distribution widths are taken to be the same, from the difference between the intercepts. This number however relies on how sensible is the quenched lattice calibration.

3.2 The low-momentum zero-crossing from ghost-loops

Another noteworthy feature taking place at very low momentum, which deserved a careful analysis in ref. [20], is the appearance of a zero-crossing and a negative logarithmic singularity at zero-momentum (many independent analyses within the SDE formalism, employing a variety of techniques and truncation schemes, have found the same in the 3-point [29–32] and the 4-point [33, 34] gluon sector, and also when light quarks are included [35]), the underlying origin of this phenomenon is the masslessness of the propagators circulating in the *nonperturbative* ghost loop diagram contributing to the SDE of n-point Green's functions [29]. Specifically, employing a nonperturbative Ansatz for the gluon-ghost vertex that satisfies the correct STI, the leading IR contribution from the ghost-loop, denoted by $\Pi_c(q^2)$, is given by [29]

$$\Pi_c(q^2) = \frac{g^2 C_A}{6} q^2 F(q^2) \int_k \frac{F(k^2)}{k^2 (k+q)^2} \,, \tag{22}$$

where C_A is the Casimir eigenvalue in the adjoint representation, and $\int_k \equiv \mu^\epsilon/(2\pi)^d \int \mathrm{d}^d k$ is the dimensional regularization measure, with $d = 4 - \epsilon$ and μ is the 't Hooft mass; evidently, in the limit $q^2 \to 0$, the above expressions behave like $q^2 \log q^2/\mu^2$. Even though this particular term does not interfere with the finiteness of $\Delta(q^2)$, its presence induces two main effects: (*i*) $\Delta(q^2)$ displays a mild maximum at some relatively low value of q^2, and (*ii*) the first derivative of $\Delta^{-1}(q^2)$ diverges logarithmically at $q^2 = 0$. The form of the renormalized gluon propagator that emerges from the complete SDE analysis

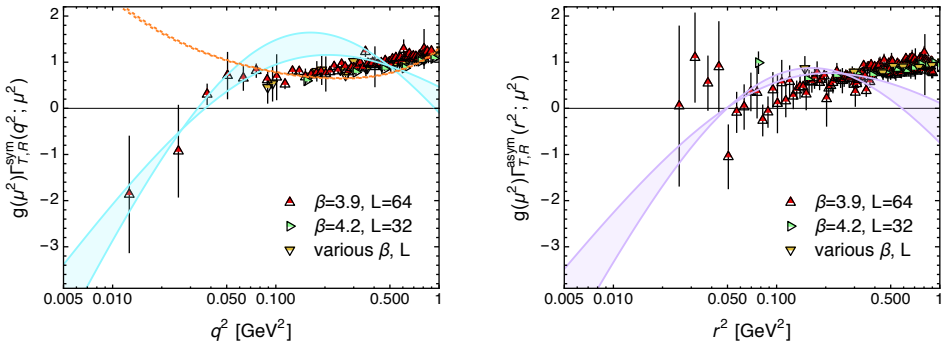

Figure 4. (color online) Comparison between the lattice results for the renormalized connected and 1-PI form factors T_R and $g\Gamma_{T,R}$ and the SDE prediction in the symmetric (left panels) and asymmetric (right panels) configurations. The band appears bounded by the results obtained with fits of (24) to lattice propagators for $L = 72$ and $L = 96$, and aims at giving an indication of the variation of the results. For the quantity $\Gamma^{\rm sym}_{T,R}$ (lower left panel) we also plot (dashed line) the semiclassical approximation derived from (19) in the previous section.

may be accurately parametrized in the IR by the expression

$$\Delta_R^{-1}(q^2;\mu^2) \underset{q^2\to 0}{=} q^2\left[a + b\log\frac{q^2+m^2}{\mu^2} + c\log\frac{q^2}{\mu^2}\right] + m^2, \tag{23}$$

with a, b, c, and m^2 suitable parameters, which captures explicitly the two aforementioned effects. Note that $\Delta_R^{-1}(0;\mu^2) = m^2$, and that the 'protected' logarithms stem from gluonic loops.

Higher order n-point functions ($n > 2$) are also affected in notable ways by the presence of ghost loops in their diagrammatic expansion[1]. Eventually, a logarithmic divergence appears, which drives the n-point funtion from positive to (infinitely) negative values, causing invariably the appearance of a zero crossing. Use of the 'background quantum' identities [36, 37], which relate background Green's functions with quantum ones, reveals that the same behavior is expected for quantum external legs, modulo a (finite) function determined by the ghost-gluon dynamics [29]. The exact position of the zero crossing is difficult to estimate, because it depends on the details of all finite contributions that are 'competing' against the logarithm coming from the ghost loop; however, it is clear that the tendency, in general, is to appear in the deep IR.

In particular, for the form factors under scrutiny, one expects the (configuration independent) IR behavior

$$\Gamma^i_{T,R}(\ell^2;\mu^2) \underset{\ell^2\to 0}{\simeq} F(0;\mu^2)\frac{\partial}{\partial\ell^2}\Delta_R^{-1}(\ell^2;\mu^2), \tag{24}$$

where $F(0) \approx 2.9$ at $\mu = 4.3$ GeV [2], which can be compared with the lattice results for the 1-PI form factors that can be obtained with the help of the relations Eqs. (5) and (8). The results are shown in Fig. 4. While it is evident that in the symmetric case a good description of the IR data is achieved, in the asymmetric case the positive excess in the data coupled to the large errors make it more difficult to discern the low momentum behavior of $T_R^{\rm asym}$ and $\Gamma^{\rm asym}_{T,R}$.

[1]We refer to ghost loops that exist already at the one-loop level. Ghost loops nested within gluon loops do not produce particular effects, because the additional integrations over virtual momenta soften the IR divergence.

There is an interesting conclusion one might draw from the behavior of these form factors. The semiclassical result based on the multi-instanton background description [19, 23] discussed in the previous section for the symmetric configuration (dashed line in the lower left panel of Fig. 4) clearly fails in accounting for the data at very deep IR momenta. This can be very well understood once we notice that at such low momenta (where the zero crossing takes place), the dynamics is entirely dominated by massless ghosts; plainly, this is a quantum effect that cannot be captured within the framework of a semiclassical approach.

4 Conclusions

Thus, we have reviewed some recent results that, relying on a very general and firm ground, strongly support that the classical solutions of the SU(3) gauge theory explain the pattern exhibited by two- and three-gluon Green functions either at low-momenta or, after the efficient killing of the UV fluctuations around the classical minima of the theory, for all momenta. The removal of UV fluctuations by the Wilson flow gets rid of the fundamental QCD scale, $\Lambda_{\rm QCD}$, introduced at the quantization level of the theory. A feature of the three-gluon Green function, taking place in its very deep IR domain, escaped to this semiclassical description: the existence of a negative logaritmic singularity at zero momentum which causes the appearance of a zero-crossing, owing to the masslessness of the ghost which contributes via nonperturbative ghost-loops in the SDE of the gluon Green's functions. This is an important phenomenon, with dynamical implications [29, 38], that can be hardly captured within the framework of a semiclassical approach.

References

[1] A. Cucchieri, T. Mendes, PoS **QCD-TNT09**, 026 (2009), 1001.2584
[2] I. Bogolubsky, E. Ilgenfritz, M. Muller-Preussker, A. Sternbeck, Phys. Lett. **B676**, 69 (2009), 0901.0736
[3] O. Oliveira, P. Silva, PoS **LAT2009**, 226 (2009), 0910.2897
[4] A. Ayala, A. Bashir, D. Binosi, M. Cristoforetti, J. Rodriguez-Quintero, Phys. Rev. **D86**, 074512 (2012), 1208.0795
[5] A.G. Duarte, O. Oliveira, P.J. Silva (2016), 1605.00594
[6] A.C. Aguilar, D. Binosi, J. Papavassiliou, Phys. Rev. **D78**, 025010 (2008), 0802.1870
[7] P. Boucaud et al., JHEP **06**, 099 (2008), 0803.2161
[8] C.S. Fischer, A. Maas, J.M. Pawlowski, Annals Phys. **324**, 2408 (2009), 0810.1987
[9] D. Dudal, J.A. Gracey, S.P. Sorella, N. Vandersickel, H. Verschelde, Phys. Rev. **D78**, 065047 (2008), 0806.4348
[10] K.I. Kondo, Phys.Rev. **D84**, 061702 (2011), 1103.3829
[11] A.P. Szczepaniak, H.H. Matevosyan, Phys. Rev. **D81**, 094007 (2010), 1003.1901
[12] P. Watson, H. Reinhardt, Phys.Rev. **D82**, 125010 (2010), 1007.2583
[13] P. Maris, C.D. Roberts, Int.J.Mod.Phys. **E12**, 297 (2003), nucl-th/0301049
[14] L. Chang, C.D. Roberts, P.C. Tandy, Chin.J.Phys. **49**, 955 (2011), 1107.4003
[15] S.x. Qin, L. Chang, Y.x. Liu, C.D. Roberts, D.J. Wilson, Phys. Rev. **C85**, 035202 (2012), 1109.3459
[16] G. Eichmann, Prog. Part. Nucl. Phys. **67**, 234 (2012)
[17] I.C. Cloet, C.D. Roberts, Prog. Part. Nucl. Phys. **77**, 1 (2014), 1310.2651
[18] D. Binosi, L. Chang, J. Papavassiliou, C.D. Roberts, Phys.Lett. **B742**, 183 (2015), 1412.4782

[19] A. Athenodorou, P. Boucaud, F. De Soto, J. Rodríguez-Quintero, S. Zafeiropoulos (2016), 1604.08887
[20] A. Athenodorou, D. Binosi, P. Boucaud, F. De Soto, J. Papavassiliou, J. Rodriguez-Quintero, S. Zafeiropoulos, Phys. Lett. **B761**, 444 (2016), 1607.01278
[21] B. Alles, D. Henty, H. Panagopoulos, C. Parrinello, C. Pittori et al., Nucl.Phys. **B502**, 325 (1997), hep-lat/9605033
[22] P. Boucaud, J. Leroy, J. Micheli, O. Pène, C. Roiesnel, JHEP **9810**, 017 (1998), hep-ph/9810322
[23] P. Boucaud, F. De Soto, A. Le Yaouanc, J.P. Leroy, J. Micheli, H. Moutarde, O. Pene, J. Rodriguez-Quintero, JHEP **04**, 005 (2003), hep-ph/0212192
[24] B. Blossier, P. Boucaud, M. Brinet, F. De Soto, X. Du, V. Morenas, O. Pene, K. Petrov, J. Rodriguez-Quintero, Phys. Rev. Lett. **108**, 262002 (2012), 1201.5770
[25] M. Luescher, JHEP **08**, 071 (2010), [Erratum: JHEP03,092(2014)], 1006.4518
[26] M. Luescher, PoS **LATTICE2013**, 016 (2014), 1308.5598
[27] E.V. Shuryak, Nucl. Phys. **B302**, 574 (1988)
[28] D. Diakonov, V.Yu. Petrov, Nucl. Phys. **B245**, 259 (1984)
[29] A.C. Aguilar, D. Binosi, D. Ibañez, J. Papavassiliou, Phys. Rev. **D89**, 085008 (2014), 1312.1212
[30] A. Blum, M.Q. Huber, M. Mitter, L. von Smekal, Phys.Rev. **D89**, 061703 (2014), 1401.0713
[31] G. Eichmann, R. Williams, R. Alkofer, M. Vujinovic, Phys.Rev. **D89**, 105014 (2014), 1402.1365
[32] A.K. Cyrol, L. Fister, M. Mitter, J.M. Pawlowski, N. Strodthoff (2016), 1605.01856
[33] D. Binosi, D. Ibañez, J. Papavassiliou, JHEP **1409**, 059 (2014), 1407.3677
[34] A.K. Cyrol, M.Q. Huber, L. von Smekal, Eur. Phys. J. **C75**, 102 (2015), 1408.5409
[35] C.T. Figueiredo, A.C. Aguilar, *Effects of divergent ghost loops in the presence of dynamical quarks*, http://sites.ifi.unicamp.br/qcd-tnt4/files/2015/08/figueiredo.pdf (2015)
[36] P.A. Grassi, T. Hurth, M. Steinhauser, Annals Phys. **288**, 197 (2001), hep-ph/9907426
[37] D. Binosi, J. Papavassiliou, Phys.Rev. **D66**, 025024 (2002), hep-ph/0204128
[38] D. Binosi, C.D. Roberts, J. Rodriguez-Quintero (2016), 1611.03523